THEORETICAL MODELS OF MAGNETIC FLUX TUBES: STRUCTURE AND DYNAMICS

O. STEINER

Kiepenheuer-Institut für Sonnenphysik, Schöneckstrasse 6, D-7800 Freiburg, FRG

Abstract. Two types of model calculations for small scale magnetic flux tubes in the solar atmosphere are reviewed. In the first kind, one follows the temporal evolution governed by the complete set of the MHD and radiative transfer equations to a (quasi) stationary solution. From such a solution the continuum contrasts of a photospheric flux tube in the visible and in the infrared continuum at 1.6 μm have been computed and are briefly discussed. The second, more empirical type of method assumes the flux tubes to be in magnetohydrostatic equilibrium. It is computationally faster and more flexible and allows us to explore a wide range of parameters. Models and insights obtained from such parameter studies are discussed in some detail. These include an explanation for the peculiar variation of the area asymmetry of Stokes V profiles across the solar disk in terms of mass motions in the surroundings of magnetic flux tubes.

Furthermore, a two-dimensional model of the lower chromosphere that has been developed is presented. Emphasis is laid on the effect of thermal bifurcation of the lower chromosphere on the structure of the chromospheric magnetic field. If the cool carbon monoxide clouds, observed in the infrared, occupy the non-magnetic regions, the flux tubes expand very strongly and form a magnetic canopy with an almost horizontal base. This has consequences for the spatial distribution of the Ca II K spectral line emission.

Finally, some consideration is given to the formation and destruction of intense magnetic flux tubes in the solar photosphere. The formation is described as a consequence of the flux expulsion process that leads to a convective instability. A possible observational signature of this mechanism is proposed.

Key words: infrared: stars – MHD – Sun: atmosphere – Sun: magnetic fields

1. Introduction

This paper concentrates on the structure of *stationary, quasi-stationary* and *static* flux tubes in the solar photosphere. A description of the dynamical formation and destruction process is given in Section 6. Emphasis is laid on observable properties of model tubes and, despite the title, formal exposition is avoided.

So far no model calculation includes the complete sequence of formation, life, and destruction of intense magnetic flux tubes. All model calculations of quasi-stationary or static magnetic flux tubes assume the existence of them at the very beginning of the calculation. This is done, for example, by the prescription of a density reduction factor which is the ratio between the density within the tube and outside it at a specified height in the atmosphere.

There exist now basically two approaches to numerical models of intense photospheric flux tubes. A first kind of calculation (Deinzer *et al.*, 1984*a*,*b*) start from a given magnetic field/plasma configuration and solve the complete set of MHD equations at subsequent time steps together with a realistic equation of state which takes partial ionization into account. By solving the equations at subsequent time steps, the solution is advanced in time and evolves away from the initial configuration to a quasi-stationary solution. This kind of calculation can be called a detailed simulation in the sense of Oran and Boris (1987). A second kind of model calculations (*e.g.*, Pizzo, 1986; Steiner *et al.*, 1986) presumes the flux tube to be

D. M. Rabin et al. (eds.), Infrared Solar Physics, 407–421.

https://doi.org/10.1017/S0074180900124672 Published online by Cambridge University Press

in magnetohydrostatic equilibrium thereby making the time stepping unnecessary. Chapter 3 and after will be devoted to this type of models.

The terms (magnetic) flux tube and flux sheet refer to models of *magnetic elements*. Magnetic elements are the tiny magnetic field concentrations which are inferred from polarimetric observations of the network and active region plages (Stenflo, 1989). They are called magnetic elements because they all show very similar physical properties, and, in a wider sense, because we think that they are the basic elements for the understanding of more global phenomena such as the heating of the chromosphere and corona, the luminosity variation with solar cycle, the thermal bifurcation in the lower chromosphere, the modification of the p-mode eigenfrequencies by magnetic fields, and activity in stellar atmospheres.

2. A Detailed Simulation

Figure 1 is the result of a detailed simulation obtained with the code originally described in Deinzer *et al.* (1984*a*). It shows contour plots of the density and temperature (*a*, *c*), magnetic lines of force (*b*), and the velocity field (*d*) of a quasi-stationary solution, resulting after having advanced the calculation through many time steps, starting from an initial flux tube configuration. The input parameters are (1) the geometrical dimension of the computational box, of which Figure 1 shows only a part, (2) the initial density reduction factor, (3) the total magnetic flux across the boundaries, and (4) the temperature at the bottom and the temperature gradient at the top boundary. The left boundary is an axis of symmetry.

The boundary conditions are chosen such that the magnetic field lines cross the upper and lower boundaries at right angles and that no magnetic flux enters nor leaves the box sideways. No material enters or leaves the box. The energy equation takes radiative transfer perpendicular to the 2-D plane of Figure 1 into account, assuming a grey medium, and incorporates a mixing length formalism for small-scale turbulent energy transport in the layers susceptible to convective instability. Since 2-D Cartesian coordinates are used, the term flux sheet is appropriate for the magnetic structure shown in Figure 1.

Since the strong magnetic pressure within the flux sheet must be balanced by the gas pressure outside it, the density within the tube is substantially lower than in the quiet atmosphere at the same geometrical height (Fig. 1*a*). This, and the reduced temperature at equal geometrical heights, have the effect that the atmosphere within the sheet is optically more transparent than the surroundings. Hence, the intense magnetic flux sheet appears as a tiny crevice in the solar atmosphere, offering a glimpse into deeper layers.

2.1. Energy Budget and Continuum Contrast

The energy budget is determined by two competing effects: suppression of convective energy transport by the strong magnetic field and lateral radiative energy influx into the tube because of the reduced opacity. The lateral radiative energy influx enforces on the external atmosphere a convective pattern as shown in Figure 1*d*. A narrow strong downflow with velocity up to 6 km s^{-1} forms in the close vicinity

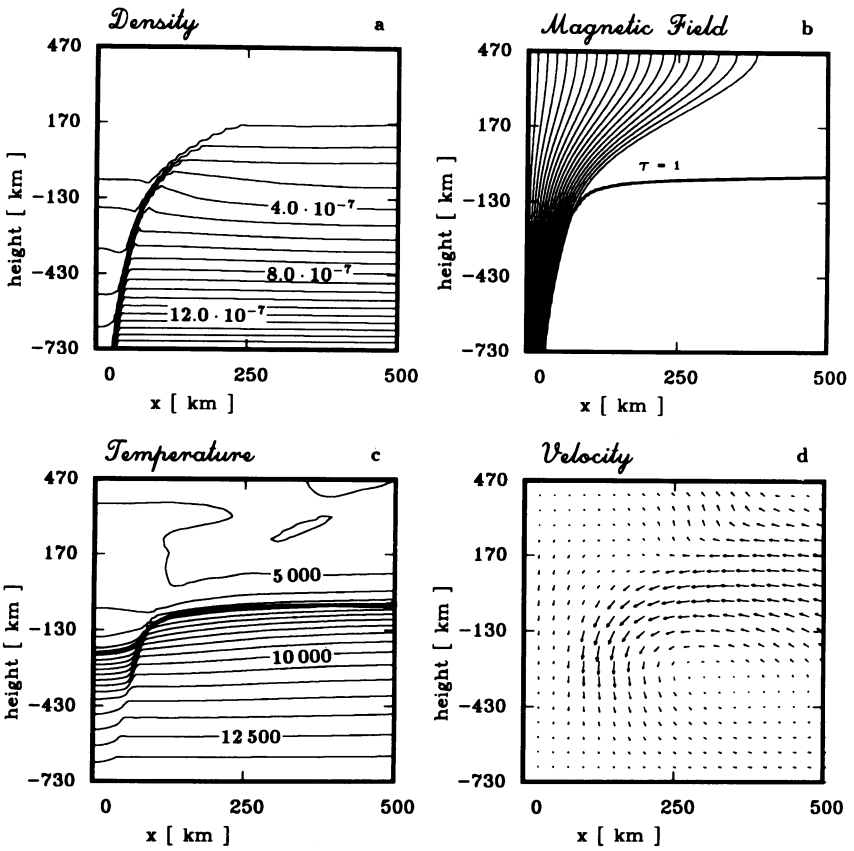

Fig. 1. Density (a) and temperature (c) contours, labeled in units of $g\,cm^{-3}$ and K, magnetic field lines (b), and velocity field (d). The maximum velocity is about 6 $km\,s^{-1}$. Courtesy M. Knölker and M. Schüssler.

of the magnetic field concentration. This mass flow is fed by a broad upflow and a horizontal flow, which, at the same time, advects the energy radiated horizontally into the flux sheet. This particular interaction of convective and radiative energy flux results in the temperature structure shown in Figure 1*c*. Due to the inhibition of convection by the strong magnetic field, the magnetic flux sheet is distinctly cooler than the surrounding atmosphere at the same *geometrical* height.

The thick curve in Figure 1*c* indicates the location at which the continuum optical depth reaches unity for an observer peering vertically down onto the structure. A close inspection shows that, if moving along this curve from the middle plane of the flux sheet outwards, the temperature is first higher, and in the close surroundings of the flux sheet boundary lower, than the temperature far away from the flux sheet. From this results the continuum appearance of the magnetic element shown in Figure 2*a* (solid curve). The "bottom" of the sheet appears bright, the peak

https://doi.org/10.1017/S0074180900124672 Published online by Cambridge University Press

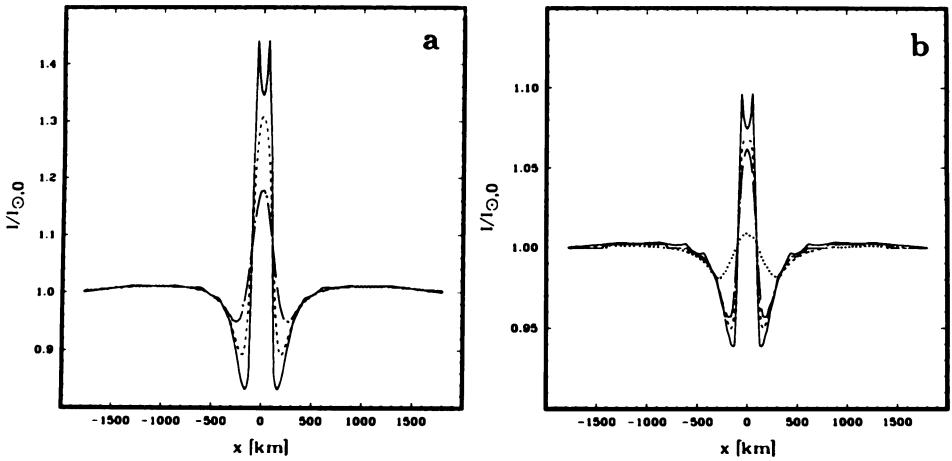

Fig. 2. *a*) Disk center continuum contrast of the flux sheet of Figure 1 at $\lambda = 5000$ Å: theoretical profile (solid), convoluted with a point spread MTF for a 0.7 m telescope (dashed), additional convolution with a seeing MTF (dot-dashed). *b*) Continuum contrast at 1.6 μm. The curves represent the theoretical profile (——), convolution with a point spread MTF for a 4 m (Super McMath) (– – ––), 2.4 m (LEST) (– · – · –), and 0.7 m (VTT) (· · · · ·) aperture. Note the different scales in Panels *a* and *b*. Courtesy M. Knölker.

values stemming from the even hotter "corners" of the depression. The magnetic element is surrounded by a dark well. The dashed curve of Figure 2*a* represents the disk center continuum contrast when a point spread modulation transfer function (MTF) for a 0.7 m telescope is applied to the theoretical contrast curve. The bright peaks then completely disappear. The dot-dashed curve results with the additional application of a seeing MTF appropriate for the German Vacuum Tower Telescope (VTT) on Tenerife.

While the positions of the isotherms in Figure 1*c* are determined by the energy budget, the $\tau = 1$ level shifts downwards when changing from the visible to the infrared continuum at 1.6 μm. The shift is different within flux sheet from the shift outside, mainly because of the difference in temperature gradient and temperature, causing a contrast profile which is different from Figure 2*a*. The theoretical disk center contrast profile at 1.6 μm is the solid curve in Figure 2*b*. If integrating over a width of 5″ a negative contrast of about -0.1% is left over compared to $+0.9\%$ in the visible. A higher spatial resolution would cut away parts of the dark well, thus leading to a positive contrast in the infrared, too (compare observations by Foukal *et al.*1990; Lin and Kuhn 1992; and Foukal and Moran 1993, in these proceedings). Figure 2*b* also shows the curves resulting after the application of a point spread MTF on the theoretical contrast curve for a 4 m (Super McMath), a 2.4 m (LEST), and a 0.7 m (VTT) aperture.

Further detailed simulations with different initial values including center-to-limb continuum contrast curves, have been published by Knölker *et al.* (1988*a*,*b*; 1991) and Grossmann-Doerth *et al.* (1989) (see also the review article by Schüssler, 1990).

3. Hydrostatic Model Flux Tubes

3.1. Basic Equations and Model Parameters

A second kind of numerical model calculation for solar magnetic flux tubes assumes hydrostatic equilibrium from the beginning. Such model calculations have been carried out for different purposes. Pizzo (1986, 1989) and Jahn (1989) have computed models of sunspots; Cally (1990) has developed a code for studies of the transition zone; and Steiner *et al.* (1986) have used this method for small scale photospheric flux tubes. The equations being solved are the force balance equation,

$$0 = -\nabla p + \rho \mathbf{g} + \mathbf{j} \times \mathbf{B} \ ,$$

Ampères law,

$$\nabla \times \mathbf{B} = 4\pi \mathbf{j} \ ,$$

and

$$\nabla \cdot \mathbf{B} = 0 \ .$$

Because the model is static, the continuity and the induction equations are absent. These equations are solved for a rotationally symmetric, untwisted, vertical flux tube.

As an example, Figure 6 shows a typical model magnetic flux tube. Within the cylindrical computational domain the nearly vertical, curving magnetic field lines delineate the flux tube, which is separated from the surrounding non-magnetic photosphere by a thin layer at which a sheet current travels in azimuthal direction. The thickness of this layer has been estimated by Schüssler (1986) and, recently, by Hirayama (1992) to 2 to 10 km. Due to the stratification of the atmosphere, the confining gas pressure, and hence the magnetic field strength, decrease with height, so that the tubes must expand to guarantee flux conservation. Ultimately, the field spreads out to fill the computational region, simulating the merging with neighboring flux tubes which prevent the tube from further expansion. Far above their merging height the flux tubes form a more or less uniform magnetic field. Inserted into the figure at several heights are curves which show the vertical and the radial magnetic field components as functions of radius.

The following parameters characterize the model: the filling factor, which is the square of the ratio of the tube radius to the width of the computational domain, the magnetic field strength, and the radius or total magnetic flux of the tube, all values specified at the height $z = 0$, where $\tau_{5000} = 1$ in the external atmosphere.

Usually the energy equation is replaced by prescribing the atmospheric structure within and outside the tube, making use of published 1-D atmospheres. This lack of self-consistency makes it possible to rapidly explore a wide range of parameters and atmospheric combinations, possibly not accessible to a detailed simulation. In addition, the computational efficiency of the present method makes it possible to derive the atmospheric structure of magnetic elements from observations of the Stokes V profiles of spectral lines.

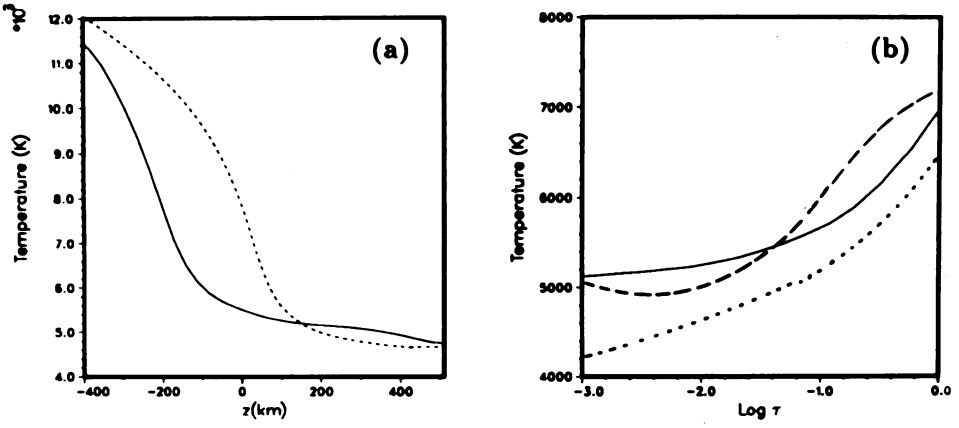

Fig. 3. Temperature as a function of geometrical height (a) and optical depth (b). The dashed curve is the result of an inversion of network Stokes V profiles, while the solid curves are the temperature along the flux sheet axis for the simulation in Figure 1. The dotted curves show the quiet-Sun model of Vernazza, Avrett and Loeser (1981). From Knölker *et al.* (1991).

3.2. Flux Tube Structure from Inversion of Stokes Spectra

Keller *et al.* (1990) made a least-squares fit to a number of characteristics of eight Fe I and two Fe II Stokes V profiles obtained from Fourier transform spectrometer observations of network and plage magnetic elements by Stenflo *et al.* (1984). By adjusting the flux-tube model parameters, they obtained the temperature as a function of $\log \tau_{5000}$, shown as the dashed curve in Figure 3*b*. The solid curve corresponds to the temperature along the axis of symmetry of the detailed model computation of Figure 1. They both are hotter than the quiet Sun model (dotted curve) at the same *optical depth*. In contrast to the optical picture, the flux tube is distinctly cooler than the quiet Sun model at the same *geometrical* height (Fig. 3*a*), with the exception of the radiatively heated upper layers. A theoretical 2-D thermal structure for the photospheric layers of magnetic flux tubes using non-grey radiative transfer has been calculated by Steiner and Stenflo (1990).

4. Stokes V Area Asymmetry

Near disk center one observes in active region plages and the quiet solar network that the area and amplitude of the blue wing of Stokes V profiles exceed those of the red wing by several percent (Solanki and Stenflo, 1984; Wiehr, 1985). At the same time, the shift of the zero-crossing wavelength is always close to zero (Solanki and Stenflo, 1986). Towards the limb the area asymmetry shows a sign reversal, *e.g.*, at $\mu = 0.4$ for the Fe I 5250.22 line (Stenflo *et al.*, 1987).

In Figure 4, a static flux tube is surrounded by a non-magnetic plasma in stationary motion. The velocity field is obtained by matching two potential flows for the upflow and the downflow region. It shows a downflow close to the flux tube

https://doi.org/10.1017/S0074180900124672 Published online by Cambridge University Press

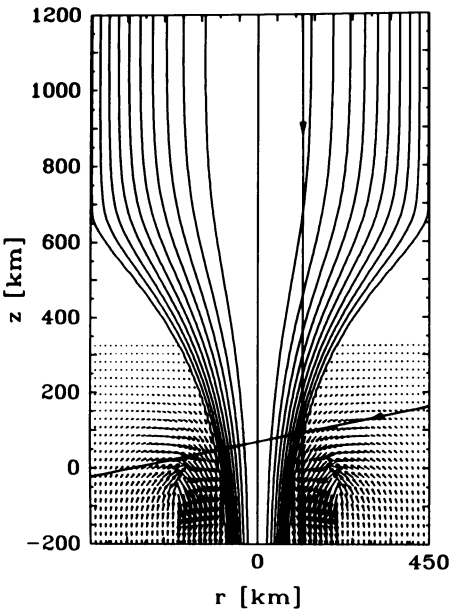

Fig. 4. Static flux tube containing the plage model atmosphere of Solanki (1986) surrounded by a non-magnetic plasma in stationary motion. The velocity field is obtained by matching two potential flows for the upflow and the downflow region. The plasma within the tube is at rest. The vertical line of sight, passes from the magnetic into the non-magnetic, down-drafting atmosphere, along which a Stokes V profile with strong area asymmetry and without shift is produced. The contributions to the area asymmetry at the two magnetic/non-magnetic interfaces of the inclined line of sight are of opposite sign.

surface (similar to Fig. 1*d*) and a granular upflow further away, crudely mimicking a simulation of granular flow (*e.g.*, Steffen, 1991). The plasma within the tube is at rest. The vertical line of sight, indicated in the Figure, passes from the magnetic into the non-magnetic, down drafting, atmosphere. This situation produces a strong Stokes V area asymmetry without shifting the zero-crossing of the profile. It can be explained by an analysis of the radiative transfer equations for polarized light (Grossmann-Doerth *et al.*, 1988, 1989). Averaging over a large number of lines of sight, weighted with the area they represent, results in Stokes V profiles may be compared with spatially unresolved spectra.

The sign of the area asymmetry depends on the sign of the expression

$$d|B|/d\tau \cdot dv(\tau)/d\tau,$$

where τ is the continuum optical depth and v the mass velocity, both along a line of sight. This expression is clearly positive for the vertical line of sight shown in Figure 4. The inclined line of sight (vertical tube close to the limb), passes two magnetic/non-magnetic interfaces for which the above expression, and hence the contributions to the area asymmetry, are of opposing sign. It therefore is not obvious

https://doi.org/10.1017/S0074180900124672 Published online by Cambridge University Press

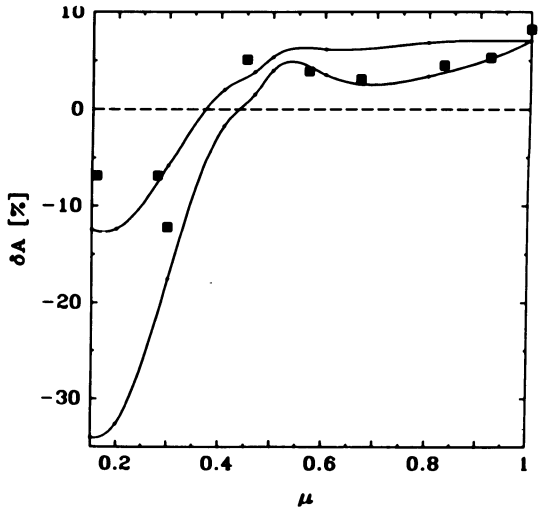

Fig. 5. Observed (squares) and calculated (curves) center-to-limb variation of the relative area asymmetry of Stokes V profiles of the Fe I 5250.22 Å line. The computed values have been obtained from the model of Figure 4 (upper curve). The lower curve results when the radial velocities are arbitrarily increased by a factor of 2.0.

what the center to limb behavior of the area asymmetry will be.

Since flux tubes cluster in network points or active region plages, Bünte *et al.* (1991) take a periodic arrangement of model flux tubes for the diagnostic procedure. Hence, close to the limb the lines of sight may pass through several flux tubes. They consider flux tubes of a field strength of 1,600 G, a diameter of 200 km, and a filling factor of 5%, all values referring to $\tau = 1$ for the external atmosphere. The diagnostic procedure is carried out for a wide range of velocity fields and temperature stratifications. These include purely vertical or purely radial motion, radial inflow and downflow, and upward and downward flow as in the example shown in Figure 4, as well as a temperature-velocity correlation to approximate a warm upflow and a cool downflow.

As the number of properties exhibited by detailed model calculations increases, such as shown in Figure 1, the center-to-limb variation (CLV) of the area asymmetry approaches the observed behavior. Observed values for the iron line 5250.22 Å as a function of $\mu = \cos\theta$ are shown in Figure 5 (filled squares), together with the results of the model data. Best agreement is obtained with the model of Figure 4, with $v_{z\,\mathrm{min}} = -4.4$ km s^{-1}, $v_{r\,\mathrm{min}} = -2.2$ km s^{-1}, and a maximum temperature excess for the upflow of 1,000 K (upper solid curve). The lower solid curve is obtained if the radial inflow is arbitrarily increased by a factor of 2.0, which demonstrates the high sensitivity of the Stokes V area asymmetry to the precise velocity field surrounding a flux tube. However, similar calculations with the Fe 5083.3 line are less satisfactory, although the sign reversal is reproduced (Bünte *et al.*, 1992).

https://doi.org/10.1017/S0074180900124672 Published online by Cambridge University Press

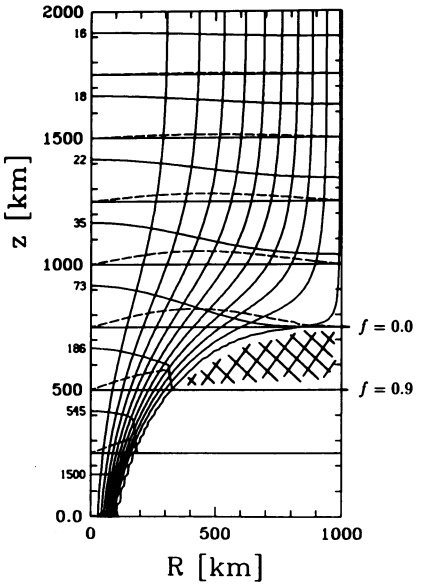

Fig. 6. Model magnetic flux tube containing the FLUXT atmosphere of Ayres *et al.* (1986) embedded in the radiative-equilibrium atmosphere of Anderson (1989). Superimposed on the field lines are horizontal curves showing the radial variation of the vertical, B_z (solid lines), and radial, B_r (dashed lines), magnetic field components at eight different heights marked by horizontal straight lines. Both, $B_z(r)$ and $B_r(r)$ are normalized to B_z at the axis, the value in Gauss of which is indicated to the left of each curve. The radius is 100 km, the field strength 1,500 G, and the filling factor 0.01; all values are specified at $z = 0$, which corresponds to $\tau_{5000} = 1$ in the external atmosphere. The hatched region indicates the location of a cool carbon monoxide cloud with a strongly height-dependent filling factor, indicated in the right margin.

5. 2-D Models for the Lower Chromosphere

Model calculations over a wide range of parameters (Steiner and Pizzo, 1989) show that, in general, the spreading of flux tubes with height is too small to form a sizable radial field component in photospheric or chromospheric layers. These are inconsistent with extensive observational investigations of Giovanelli and Jones (Giovanelli, 1980; Giovanelli and Jones, 1982; Jones and Giovanelli, 1983; Jones, 1985), which invariably show magnetic canopies extending as low as in the upper photosphere. We have found that canopy fields originating from intense photospheric flux tubes can only be obtained if the flux tubes are embedded in a cool atmosphere, while the chromospheric temperature rise is present only within the flux tubes (Solanki and Steiner, 1990). The crucial point is that the gas pressure in the cool, non-magnetic atmosphere decreases rapidly to a value close to the pressure within the tube, at which height the field is forced to spread nearly horizontally, thereby forming a magnetic canopy.

An example of such a model is shown in Figure 6. The flux tube contains the

https://doi.org/10.1017/S0074180900124672 Published online by Cambridge University Press

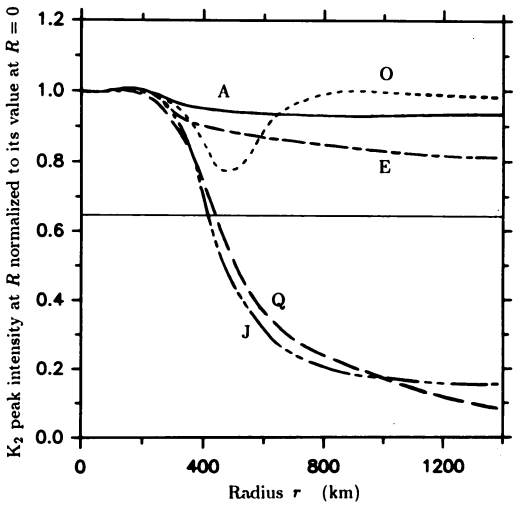

Fig. 7. Intensity of the Ca II K_2 peak with radius r, normalized to the intensity at the flux tube axis ($r = 0$) for different atmospheric model combinations. The horizontal line marks the value to which the K_2 intensity drops at large r according to observations of Grossmann-Doerth *et al.* (1974). From Solanki *et al.* (1991).

plage flux tube atmosphere FLUXT of Ayres *et al.* (1986) and is embedded in the radiative equilibrium model of Anderson (1989). The Anderson atmosphere shows a dramatic temperature drop above the classical temperature minimum, due to the formation of carbon monoxide. The tube shows a sizable radial field component and merges with neighboring flux tubes at a height of only 800 km above $\tau = 1$ of the external atmosphere. Other atmospheric combinations, including the empirical cool atmosphere of Ayres *et al.* (1986) result in merging heights between 800 to 1,200 km.

In this picture the much debated carbon monoxide cloud (Ayres 1991 and Ayres 1993, in these proceedings) occupies the hatched region of Figure 6. A shortcoming of the present model is the temperature discontinuity at the flux tube boundary which sharply delineates the CO cloud. Full 2-D radiative transfer is needed to obtain a smooth transition. Note, however, the strongly height-dependent filling factor of the CO cloud, which must have a distinct effect on the center-to-limb behavior of the CO lines. This model suggests that a high-resolution filtergram in the 4.7 μm CO lines would depict the CO clouds in quiet supergranular centers. However, according to Figure 6, they are rather shallow, so that disk center observations are probably not suitable. Furthermore, the lines would not be affected by any Zeeman splitting or broadening because they would be formed in field free regions.

The present model has other advantages besides the ability to incorporate the CO cloud and to form a relatively low lying magnetic canopy. Solanki *et al.* (1991) showed that it also may explain the spatial scale and amplitude of the horizontal Ca II K_2 intensity variation in the quiet Sun. These authors computed synthetic Ca II K spectral lines along many vertical lines of sight across models with different

https://doi.org/10.1017/S0074180900124672 Published online by Cambridge University Press

flux tube atmospheres surrounded by Ayres's (1986) empirical cool atmosphere. It turned out that the source function for this line is very sensitive to the height extent of the cool atmosphere, which in turn is limited by the base field strength of the magnetic canopy. Strong Ca II K core emission is always present for rays close to the axis of symmetry of the tube, while rays passing through the canopy may fail to show any core emission at all. This situation is reflected in Figure 7, which shows the Ca II K_2 peak intensity across the radius of flux tubes with a moderate chromospheric temperature rise (curves J and Q) and a strong temperature rise (A and E). Models J and Q show a Ca II K grain size of about 1″, in agreement with the observational values of Cram and Damé (1983). If the temperature profiles of the upper layers of the flux-tube atmosphere lie between those of the plage models VALP of Ayres *et al.* (1986) (model E) and VALF of Vernazza *et al.* (1981) (model J), the curve can be expected to drop to the indicated observed value and, at the same time, the average profile over the radius would then best reproduce the Ca II K spectral line of the average quiet Sun.

6. Formation and Destruction of Intense Magnetic Flux Tubes and a Possible Infrared Signature

6.1. Flux Expulsion and Convective Collapse

Two mechanisms have been proposed for the concentration of magnetic flux into structures of high field strength: flux expulsion and convective collapse. Flux expulsion is the process of field advection by the granular and supergranular velocity field, which expels the magnetic flux from the cell interiors into the narrow intergranular lanes. The order of magnitude of the field strength resulting from this process is the equipartition field strength

$$\frac{B_{\mathrm{eq}}^2}{8\pi} = \frac{\rho}{2} v^2 \ ,$$

where ρ is the density and v the typical granular velocity, both at the solar surface. It results in an equipartition field strength of $B_{\mathrm{eq}} \approx 400$ G close to the solar surface.

Flux expulsion by convective flows have been investigated numerically in the kinematic as well as in the dynamic case (*e.g.*, Proctor and Weiss, 1982; Hurlburt and Toomre, 1988). Figure 8 shows four snapshots of a flux expulsion simulation in a compressible, stratified medium, similar to an example of Hurlburt and Toomre, 1988. The computation has been started with a homogeneous vertical field. The temperature at the top and the temperature gradient at the bottom are prescribed. The ratio of the initial density at the bottom to that at the top is 5. The Rayleigh number is far above critical, so that magnetoconvection sets in. The flux expulsion process leads to particularly strong field concentration in the downflow region of the cells.

However, field concentration by the expulsion process is insufficient to explain the kG fields of magnetic elements. As a consequence of the flux expulsion process the growing magnetic field concentration causes the retardation of the horizontal flow towards the downflow region. This leads to a cooling of the magnetic region,

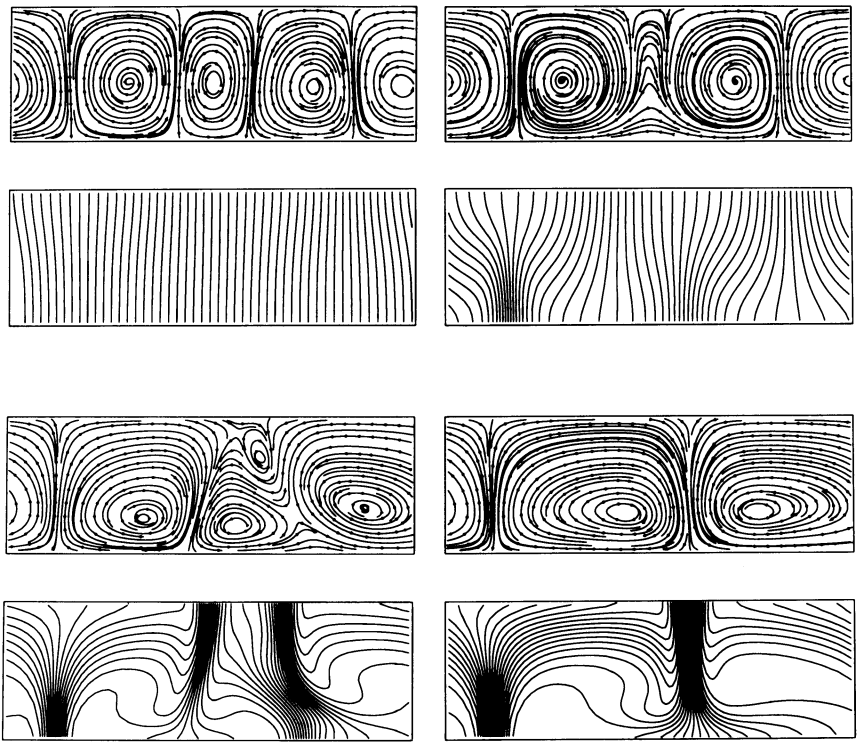

Fig. 8. Four snapshots of the numerical simulation of flux expulsion in a compressible, stratified medium, similar to Hurlburt and Toomre (1988). The top panel shows streak lines of the mass motion, the bottom panel magnetic lines of force. Starting with a homogeneous, vertical magnetic field the flow evolves to a stationary pattern with the field concentrated to equipartition strength in the downflow region.

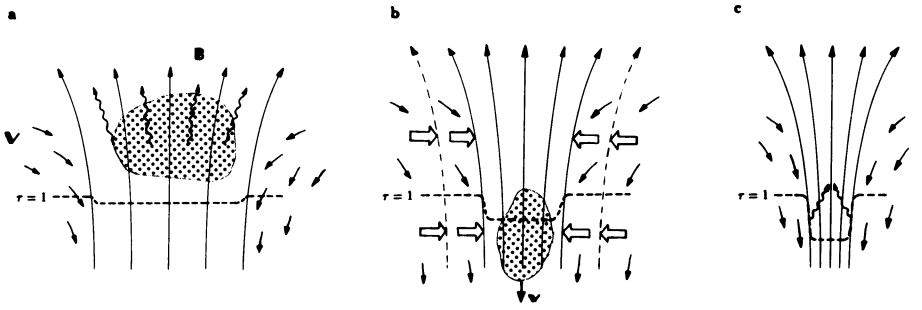

Fig. 9. Schematic sketch of the formation of an intense magnetic flux tube by means of the convective collapse. The dotted cloud represents an arbitrary material package. Short thin arrows indicate plasma motion, whereas the long, vertically oriented arrows represent field lines. The wavy arrows signify radiative energy losses and the bold arrows in the middle sketch stand for the fast magnetic field concentration by the convective collapse.

https://doi.org/10.1017/S0074180900124672 Published online by Cambridge University Press

because the radiative losses can no longer be replenished by the throttled horizontal flow (Fig. 9). This cooling effect causes an increase in the magnetic field, since the gas pressure decreases and leads to a downflow. Provided that an adiabatic downflow in the thermally isolated flux tube takes place in a superadiabatically stratified environment, an instability ensues, known as the convective collapse. This causes a partial evacuation of the tube and leads to a magnetic field which is confined by the external gas pressure and hence of the order of $B \approx (8\pi p_{\rm ext})^{1/2}$. This formation scenario is described in greater detail by Schüssler (1992) with a complete list of references on the subject.

6.2. Can Convective Collapse be Observed?

While the convective collapse phenomenon has been studied in detail with analytical and numerical methods (see Schüssler, 1992 and references therein), there have been no direct or indirect observations of it, heretofore.

I propose that the key to a possible detection of a convective collapse is the strong splitting of Zeeman sensitive lines in the infrared (*e.g.*, Fe I 1.5648 μm, $g = 3$). This seems to be the only means to directly observe intrinsically weak photospheric fields of the order of the equipartition field strength (Rüedi *et al.*, 1992; Stenflo, 1992; Solanki 1993, in these proceedings). In the visible, the detection of weak fields is difficult, since the Zeeman broadening is dominated by velocity broadening.

The convective collapse lasts at most a few minutes. Therefore, a time resolution of about ten seconds is needed. The shortness of the process dictates the selection of a location on the Sun with high probability for the occurrence of a collapse, such as a flux-emergent region. Because of the fast field concentration in the course of the convective collapse, we expect to observe a sudden rise of field strength at a location where a magnetic flux density of the order of equipartition strength has been measured previously. More precisely, a quick increase of the peak separation of the infrared Stokes V profiles should be observed. At the same time, due to the adiabatic downflow within the forming flux tube, the Stokes profiles are shifted to the red. However, this shift should disappear in the final, stationary state of the flux tube. A variation in Stokes V amplitude may occur rather because of the increasing temperature of the downshifting material than because of the increasing field strength, since the equipartition field already almost saturates the Stokes V profiles in the infrared (Solanki, private communication).

In real observations, however, the magnetic flux density within the finite spatial resolution element may vary strongly or change sign and not all magnetic flux may become involved in the convective collapse. A mixture of weak and strong field components is expected to be present after the collapse. This gives rise to peculiar Stokes V profiles (Rüedi *et al.*, 1992), so that the interpretation of the observation may not be as straightforward as described above. The magnetohydrodynamic simulation of the convective collapse, together with the computation of synthetic infrared Stokes profiles, will probably be most useful for the understanding and interpretation of such observations.

6.3. A Destruction Mechanism for Magnetic Flux Tubes

Small scale magnetic flux tubes with a total magnetic flux of typically a few times 10^{18} Mx are susceptible to the interchange (flute) instability. Schüssler (1984) has shown that thin flux tubes can be stable if they are surrounded by a whirl flow. Bünte *et al.* (1992) and Bünte *et al.* (1993), in these proceedings) found that an azimuthal velocity component of up to 4 $\mathrm{km\,s^{-1}}$ is needed, depending on the atmospheric structure of the flux tube and its close surroundings, to prevent interchange instability. This value refers to the flux tube surface at a depth of about 100 km below the $\tau_{5000} = 1$ level.

Whirl flows are expected to arise from the "bathtub effect" in granular downdrafts which are a natural location of magnetic flux tubes. Moreover, as seen from Figure 1, the mere existence of a magnetic flux tube leads to the formation of converging downflows in its close surroundings which may survive even if the granular pattern changes. However, a strong perturbation may cause the disruption of the whirl flow and hence give way to the flute instability. This MHD instability induces a shredding of the flux tube possibly leading to its disappearance by a flux rearrangement within a few minutes.

Acknowledgements

I am very grateful to M. Schüssler for critically commenting on and carefully reading the manuscript. I also wish to thank M. Knölker for Figures 1 and 2 and M. Bünte for Figures 4 and 5. This work has been supported by the Deutsche Forschungsgemeinschaft under grant SCHU 500/6-1.

References

Anderson, L. S.: 1989, *Astrophys. J.* **339**, 558.
Ayres, T. R.: 1991, in P. Ulmschneider *et al.* (eds.), *Mechanisms of Chromospheric and Coronal Heating*, Springer-Verlag, p. 228.
Ayres, T. R.: 1993, these proceedings.
Ayres, T. R., Testerman, L., Brault, J. W.: 1986, *Astrophys. J.* **304**, 542.
Bünte, M., Solanki, S. K., Steiner, O.: 1992, *Astron. Astrophys.*, submitted.
Bünte, M., Steiner, O., Solanki, S. K.: 1991, in L. J. November (ed.), *Solar Polarimetry*, National Solar Observatory, Sunspot, New Mexico, p. 468.
Bünte, M., Steiner, O., Pizzo, V. J.: 1992, *Astron. Astrophys.*, submitted.
Bünte, M., Steiner, O., Solanki, S. K., Pizzo, V. J.: 1993, these proceedings.
Cally, P. S.: 1990 *J. Comput. Phys.* **93**, 411.
Cram, L. E., Damé, L.: 1983, *Astrophys. J.* **272**, 355.
Deinzer, W., Hensler, G., Schüssler, M., Weisshaar, E.: 1984*a*, *Astron. Astrophys.* **139**, 426.
Deinzer, W., Hensler, G., Schüssler, M., Weisshaar, E.: 1984*b*, *Astron. Astrophys.* **139**, 435.
Foukal, P., and Moran, T.: 1993, these proceedings.
Foukal, P. Little, R., Graves, J., Rabin, D., Lynch, D.: 1990, *Astrophys. J.* **353**, 712.
Giovanelli, R. G.: 1980, *Solar Phys.* **68**, 49.
Giovanelli, R. G., Jones, H. P.: 1982, *Solar Phys.* **79**, 267.
Grossmann-Doerth, U., Kneer, F., von Uexküll, M.: 1974, *Solar Phys.* **37**, 58.
Grossmann-Doerth, U., Schüssler, M., Solanki, S. K.: 1988, *Astron. Astrophys.* **206**, L37.
Grossmann-Doerth, U., Knölker, M., Schüssler, M., Weisshaar, E.: 1989, in R. J. Rutten and G. Severino (eds.), *Solar and Stellar Granulation*, NATO ASI Series, Vol. **263**, Kluwer, Dordrecht, p. 481.
Grossmann-Doerth, U., Schüssler, M., Solanki, S. K.: 1989, *Astron. Astrophys.* **221**, 338.

Hirayama, T.: 1992, *Solar Phys.* **137**, 33.
Hurlburt, N. E., Toomre, J.: 1988, *Astrophys. J.* **327**, 920.
Jahn, K.: 1989, *Astron. Astrophys.* **222**, 264.
Jones, H. P.: 1985, in B. W. Lites (ed.), *Chromospheric Diagnostics and Modelling*, National Solar Observatory, Sunspot, New Mexico, p. 175.
Jones, H. P., Giovanelli, R. G.: 1983, *Solar Phys.* **87**, 37.
Keller, C. U., Solanki, S. K., Steiner, O., Stenflo, J. O.: 1990, *Astron. Astrophys.* **233**, 583.
Knölker, M., Schüssler, M.: 1988, *Astron. Astrophys.* **202**, 275.
Knölker, M., Schüssler, M., Weisshaar, E.: 1988, *Astron. Astrophys.* **194**, 257.
Knölker, M., Grossmann-Doerth, U., Schüssler, M., Weisshaar, E.: 1991, *Adv. Space Res.* **11**, (5)285.
Lin, H., Kuhn, R.: 1992, *Solar Phys.* **141**, 1.
Oran, E. S., Boris, J. P.: 1987, *Numerical Simulation of Reactive Flow*, Elsevier, New York.
Pizzo, V. J.: 1986, *Astrophys. J.* **302**, 785.
Pizzo, V. J.: 1990, *Astrophys. J.* **365**, 764.
Proctor, M. R. E., Weiss, N. O.: 1982, *Rep. Prog. Phys.*, **45**, 1317.
Rüedi, I., Solanki, S. K., Livingston, W. C., Stenflo, J. O.: 1992, *Astron. Astrophys.* **263**, 323.
Schüssler, M.: 1984, *Astrophys. J.* **140**, 453.
Schüssler, M.: 1986, in Deinzer *et al.* (eds.), *Small Scale Magnetic Flux Concentrations in the Solar Photosphere*, Vandenhoeck and Ruprecht, Göttingen, p. 127.
Schüssler, M.: 1990, in J. O. Stenflo (ed.), 'Solar Photosphere: Structure, Convection, and Magnetic Fields', *Proc. IAU Symp.* **138**, 161.
Schüssler, M.: 1992, in J. T. Schmelz and J. C. Brown (eds.), *The Sun – a Laboratory for Astrophysics*, NATO Advanced Study Institute, Kluwer, Dordrecht, in press.
Solanki, S. K.: 1986, *Astron. Astrophys.* **168**, 311.
Solanki, S. K.: 1987, *Ph.D. Thesis*, ETH Zürich.
Solanki, S. K.: 1993, these proceedings.
Solanki, S. K., Stenflo, J. O.: 1984, *Astron. Astrophys.* **140**, 185.
Solanki, S. K., Steiner, O.: 1990, *Astron. Astrophys.* **234**, 519.
Solanki, S. K., Steiner, O., Uitenbroek, H.: 1991, *Astron. Astrophys.* **250**, 220.
Steffen, M.: 1991, in L. Crivellari *et al.* (eds.), *Stellar Atmospheres: Beyond Classical Models*, NATO ASI Series, Vol. **341**, Kluwer, Dordrecht, p. 247.
Steiner, O., Pizzo, V. J.: 1989, *Astron. Astrophys.* **211**, 447.
Steiner, O., Stenflo, J. O.: 1990, in J. O. Stenflo (ed.), 'Solar Photosphere: Structure, Convection, and Magnetic Fields', *Proc. IAU Symp.* **138**, 181.
Steiner, O., Pneuman, G. W., Stenflo, J. O.: 1985, *Astron. Astrophys.* **170**, 126.
Stenflo, J. O.: 1989, *Astron. Astrophys. Rev.* **1**, 3.
Stenflo, J. O.: 1992, in D. S. Spicer (ed.), *Electromechanical Coupling of the Solar Atmosphere*, Proc. OSL Workshop, Capri, Italy, Amer. Inst. Phys., in press.
Stenflo, J. O., Harvey, J. W., Brault, J. W., Solanki, S. K.: 1984, *Astron. Astrophys.* **131**, 33.
Stenflo, J. O., Solanki, S. K., Harvey, J. W.: 1987, *Astron. Astrophys.* **171**, 305.
Vernazza, J. E., Avrett, E. H., Loeser, R.: 1981, *Astrophys. J. Suppl.* **45**, 635.
Wiehr, E.: 1985, *Astron. Astrophys.* **149**, 217.